PHYSICAL REVIEW E **96**, 010402(R) (2017)

Phenomenological modeling of durotaxis

Guangyuan Yu,[1,2] Jingchen Feng,[2] Haoran Man,[1] and Herbert Levine[2,3,*]
[1]*Physics and Astronomy Department, Rice University, Houston, Texas 77005, USA*
[2]*Center for Theoretical Biological Physics, Rice University, Houston, Texas 77005, USA*
[3]*Department of Bioengineering, Rice University, Houston, Texas 77005, USA*
(Received 21 February 2017; revised manuscript received 26 May 2017; published 17 July 2017)

Cells exhibit qualitatively different behaviors on substrates with different rigidities. The fact that cells are more polarized on the stiffer substrate motivates us to construct a two-dimensional cell with the distribution of focal adhesions dependent on substrate rigidities. This distribution affects the forces exerted by the cell and thereby determines its motion. Our model reproduces the experimental observation that the persistence time is higher on the stiffer substrate. This stiffness-dependent persistence will lead to durotaxis, the preference in moving towards stiffer substrates. This propensity is characterized by the durotaxis index first defined in experiments. We derive and validate a two-dimensional corresponding Fokker-Planck equation associated with our model. Our approach highlights the possible role of the focal adhesion arrangement in durotaxis.

DOI: 10.1103/PhysRevE.96.010402

Cells are capable of sensing and responding to the mechanical properties of their external environment. For example, cytoskeletal stiffness [1], cellular differentiation [2–5], and cell morphology and motility [6–9] are all strongly influenced by extracellular matrix stiffness. In particular, it has been shown experimentally that cells prefer crawling towards the stiffer parts on substrates with spatially varying rigidity, a property that is referred to as durotaxis. Durotaxis is a universal property of motile cells, despite the diverse shapes and structures among different cell types. It has been proposed that durotaxis is critical for fine-tuning cell path finding and wound healing [10,11]. Also, there is increasing evidence showing that durotaxis is involved in cancer metastasis, since tumors are usually stiffer than the surrounding materials [12,13].

A standard approach to modeling cell motility is to assume that cells execute a persistent random walk [14–16]; sometimes Lévy walks are used instead [17,18]. Recently, Novikova *et al.* applied persistent random-walk ideas to understand durotaxis by relating persistence to substrate stiffness [19]. Their approach did show how this assumption could lead to durotaxis, but did not propose any direct mechanical reason for this correspondence; also they did not fully analyze their model in the relevant case of a two-dimensional (2D) spatial domain. In this study, we propose a simple intracellular mechanism that naturally leads to stiffness-dependent persistence that, in agreement with the above findings, results in durotaxis. Our approach combines direct simulations with the derivation of a quantitatively accurate 2D Fokker-Planck equation, for which the numerical solution matches well with simulation data.

Our basic hypothesis is built on the fact that cells are observed to be more polarized when they move on stiffer materials. Cells have sophisticated mechanisms to sense stiffness, involving various cellular components and subsystems including the plasma membrane [20,21], actin filaments [22,23], actomyosin-based contractility, integrin-based focal adhesions [24,25], etc. Once cells sense a stiffer substrate, they take on a more elongated shape [26,27] as a response. Now cells move by protrusions that occur with the help of focal adhesions that allow force transmission to the substrate. We will assume that the change in shape to being more polarized implies that focal adhesions (FAs) are formed within a narrower wedge on the cell front. In other words, we assume that the FA distribution is correlated with cell polarization; the exact biophysical process that creates this correlation is not addressed here. It is also possible that the total number of FAs present at some fixed time increases on stiffer substrates, as FAs are observed to be more stable on stiffer substrates [6]. In our model, both the distribution and the total number of FAs directly control the variance of deflection angles in cell motion over a short-time interval. We also consider the possibility that cell speed may also depend on stiffness. These mechanisms will create the necessary relationship between stiffness and persistence.

In experiments, the locations of cells moving on a 2D surface are typically recorded at fixed time intervals. Accordingly, we model the cell as a rigid object moving with velocity v and rotating its motion direction Φ (its polarization) by an angle $\Delta\Phi$ at fixed time intervals $\Delta t = t_{i+1} - t_i$, which we take to be our unit of time. To determine $\Delta\Phi$, we assume that there are a number N_f of focal adhesions that are positioned at distances r_i from the cell center and angles θ_i relative to the current direction of motion; these are chosen randomly from uniform distributions with ranges $(r_{\min}, r_{\max})$ and $(-\theta_{\max}, \theta_{\max})$, respectively. We assume, in line with the previous arguments, that $\theta_{\max}$ is determined by local substrate stiffness k as $\theta_{\max} = A/k$, where A is a constant factor. The basic picture of our cell is given in Fig. 1. Our calculations will assume that N_f remains constant. The driving force from each focal adhesion is assumed to have a constant magnitude and to point in the current moving direction. The net driving force is canceled by the friction acting on the cell, thereby determining the velocity. It is worth noting that in reality, FAs are located at both the front and the back of the cell. The forces applied by back FAs, which typically operate in a slipping rather than gripping mode [28], are replaced with friction.

At each time step, the dynamical formation and disruption of FAs cause a possible imbalance in the driving torque. With fast relaxation, the cell will rotate by an angle $\Delta\Phi$ at each time step to satisfy zero net torque

$$\sum_{i=1}^{N_f} r_i \sin(\theta_i - \Delta\Phi) = 0, \tag{1}$$

*Corresponding author: herbert.levine@rice.edu

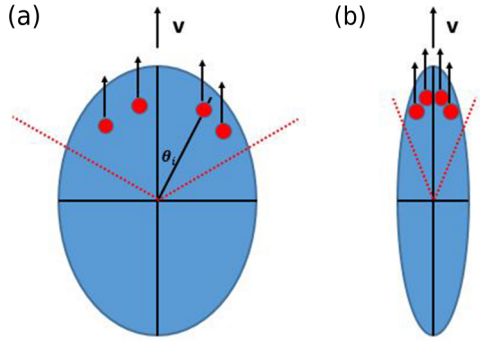

FIG. 1. Sketch of our model. Red circles represent focal adhesions. In our simulation, focal adhesions are randomly generated within an angular range bounded by red lines in the figure at each step. (a) For cells on a soft substrate, the distribution of FAs is relatively wide. (b) Conversely, for cells on a hard substrate, the distribution of FAs is relatively narrow.

whose solution is

$$\tan\Delta\Phi = \frac{\sum_{i=1}^{N_f} r_i \sin(\theta_i)}{\sum_{i=1}^{N_f} r_i \cos(\theta_i)}. \tag{2}$$

For the purpose of illustration, we typically set $r_i = 1$ for all i and $N_f = 12$ in our model.

Clearly, the variance of the induced distribution for $\Delta\Phi$ determines the persistence of the motion. Here we use a Monte Carlo sampling method to evaluate this variance. We use 10^6 sampling steps and have checked that this gives us an accurate evaluation for the range of parameters we have investigated. For the case of fixed radii, we obtain

$$\int\cdots\int_{-\theta_{\max}}^{\theta_{\max}} \left(\prod_{i=1}^{N_f} \frac{d\theta_i}{2\theta_{\max}}\right) \arctan^2\left(\frac{\sum_{i=1}^{N_f}\sin(\theta_i)}{\sum_{i=1}^{N_f}\cos(\theta_i)}\right).$$

One can also compute the variance for the more general situation with a distribution for the radii as well. Typical results of this calculation are shown in Fig. 2(a). For use later on, we have fitted the data for the case $N_f = 12$ with fixed radii to a simple function of k,

$$\sigma(k) = \frac{1}{\alpha k + \beta}. \tag{3}$$

As expected, increasing N_f or decreasing $\theta_{\max}$ reduces the variance, whether directly or via more averaging. Thus, rigidity-dependent changes in the focal adhesion dynamics can indeed be used to model the mechanism underpinning the persistence-stiffness correlation.

Since focal adhesions are dynamically formed and destroyed, in our model at each time step the locations of all focal adhesions θ_i are reselected with no correlation to their previous value, hence $\langle\Delta\Phi(t_i)\Delta\Phi(t_{i+1})\rangle = 0$. Thus, on a uniform substrate, approximating the distribution of $\Delta\Phi$ to be Gaussian with the calculated width reduces our model to a version of the wormlike chain, where the mean-square displacement is

$$\langle x^2\rangle = v^2\tau_p^2\left(\frac{t}{\tau_p} + e^{-t/\tau_p} - 1\right). \tag{4}$$

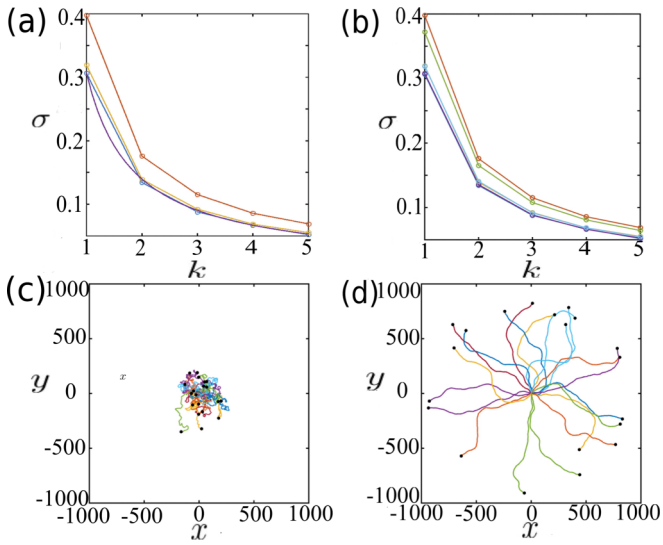

FIG. 2. Simulation result of uniform substrates and the variance of deflected angles. (a) Variance of deflected angles calculated by Monte Carlo sampling for σ^2 vs stiffness k, with $N = 8$ and $r_i = 1$ (red), $N = 12$ and $r_i = 1$ (blue), $N = 12$ and $r_i \in (0.5,1.5)$ (yellow) for all i and the fitted function $\sigma(k)$ with $\alpha = 3.9$ and $\beta = -0.645$ [Eq. (3)] (purple). (b) Comparison between Monte Carlo sampling and direct simulation for $N = 12$ and $r = 1$ (red), with two lines overlapping as the purple line; for $N = 12$ and $r_i \in (0.5,1.5)$, with two lines overlapping as the blue line; for $N = 8$ and $r_i = 1$, shown by the green line (direct simulation); and for $N = 8$ and $r_i = 1$, shown by the red line (Monte Carlo sampling). (c) and (d) Simulation of 1000 time steps with $v = 1$ (arbitrary units). The initial position of 20 cells is (0,0) and the initial moving direction is randomly selected. The black dots are the final positions of each cell. (c) On a soft substrate, $k = 1$ and $\theta_i \in (-0.5\pi, 0.5\pi)$ for all i. (d) On a stiff substrate with $k = 5$, the angle range is $\theta_i \in (-0.1\pi, 0.1\pi)$ for all i.

Here the persistence time is defined as $\tau_p = -\frac{\Delta t}{\ln\langle\cos\Delta\Phi\rangle}$. Since $\langle\cos\Delta\Phi\rangle = e^{-\sigma^2\Delta t/2}$, where $\sigma^2\Delta t = \mathrm{Var}(\Delta\Phi)$, $\tau_p = \frac{2}{\sigma^2}$. In terms of real numbers, for example, from Ref. [18], we can set $v = 0.5\ \mu$m (per δt) and $\delta t = 0.01h$. We then obtain $\sigma^2\delta t \sim 0.05^2$ on stiff substrates and $\sim 0.3^2$ on soft substrates. In this way, we find $\tau_p = 2/\sigma^2 \sim 0.2h$ on soft substrates and $\sim 8h$ on stiff substrates in our simulations.

Initially, we assume that the cell speed v is stiffness independent and we simulate cell trajectories on uniform substrates with different stiffness and verify the previous results for σ^2 [see Fig. 2(b)]. In Figs. 2(c) and 2(d) we show trajectories of cells simulated on both uniform soft and hard substrates. Consistent with the experimental observation [29], cells crawl more efficiently on stiffer substrates.

Next we study the effect of stiffness gradients on cell motility. We impose a constant stiffness gradient in the central region with constant low stiffness k_{left} on the left side and high stiffness k_{right} on the right side. We fix both k_{left} and k_{right} and vary the width of the central region

$$k(x) = \begin{cases} k_{\text{left}} = 1, & -1000 < x < -L \\ k_{\text{left}} + \frac{k_{\text{right}} - k_{\text{left}}}{2L}(X + L), & -L \leqslant X \leqslant L \\ k_{\text{right}} = 5, & L < x < 1000. \end{cases} \tag{5}$$

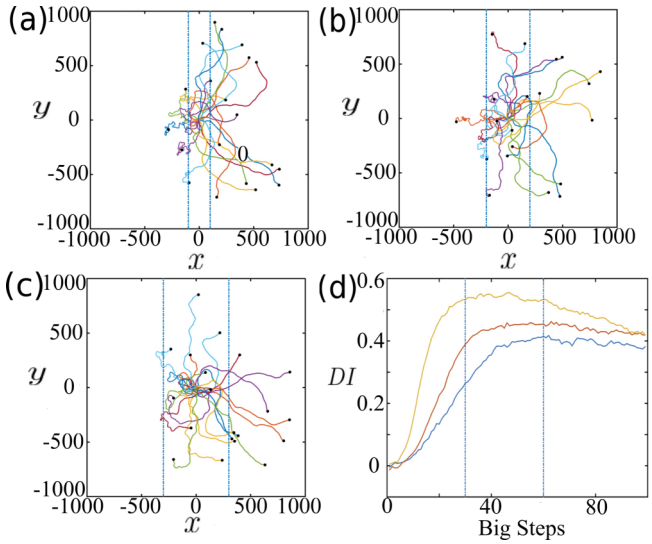

FIG. 3. Direct simulation on the gradient matrix and DI. (a)–(c) Soft substrate $k = 1$ in the left region and hard substrate $k = 5$ in the right region. The central region has a constant gradient stiffness and varying width: (a) $L = 100$, (b) $L = 200$, and (c) $L = 300$ (arbitrary units). (d) Durotaxis indices at several values of L; the index decreases as L is increased. Every ten steps is counted as a big step.

Initially, all our cells are placed at the origin and given a random initial direction. For small width, at a time when half of the cells go into the stiff region on the right, the other half are still hovering within the central gradient region [Fig. 3(a)]. As the width increases, fewer and fewer cells enter the soft region on the left [Figs. 3(b) and 3(c)]. This is caused by the fact that larger width allows more moving steps inside the gradient region and cells have more time to adapt to the direction of stiffness gradient. We further characterize these results by the durotaxis index (DI) [29]. We calculate DI defined below every ten time steps in our simulation:

$$\mathcal{D}(t_i) = \frac{N_{\text{right}} - N_{\text{left}}}{N_{\text{right}} + N_{\text{left}}}, \tag{6}$$

where N_{right} and N_{left} are the number of cells having positive and negative net displacement in the x direction, respectively. This index is in the range $[-1,1]$. Larger durotaxis indices indicate that more cells are moving towards the ascending gradient direction.

We find that the curve can be divided into three sections [Fig. 3(d)]. In the first section, nearly all cells are still in the gradient region. The index increases rapidly, which suggests that cells start being guided by the stiffness gradient. Consistent with experiment observation [27], the magnitude of the DI is highly correlated with the magnitude of the gradient. In the second section, part of the cells are in the gradient region while the other have entered the uniform stiffness region. In the last section, the index starts decreasing because all cells move into the uniform rigid region and begin to execute random walks. The DI curve in the first section elucidates the role of gradient stiffness on cell motility.

To facilitate understanding of our simulation data, we now develop a Fokker-Plank equation for the probability distribution $P(x,y,\Phi;t)$ governing a population of particles in our model. We will be specifically interested in cases with a stiffness gradient, which we choose to lie along the x direction. We focus on the variation with x and Φ and introduce $p = \int dy\, P$ as a two-dimensional density. For any single cell, the next position $x(t + dt)$ depends on the current position and angle via $x(t) + v\cos[\Phi(t)]dt$. We can therefore represent a single step in our stochastic process via

$$p(x,\Phi;t+dt) = \int_0^{2\pi} p(x - v\cos(\Phi_0)dt, \Phi_0; t) \times f(x - v\cos(\Phi_0)dt, \Phi_0 - \Phi)d\Phi_0, \tag{7}$$

where we will use the aforementioned Gaussian approximation

$$f(x,\Phi_0 - \Phi) = a(x)e^{-(\Phi_0-\Phi)^2/2\sigma(x)^2 dt}. \tag{8}$$

Here $a(x) = \sqrt{\frac{1}{2\pi\sigma(x)^2 dt}}$ is the normalization coefficient as long as the width is significantly smaller than 2π. Note that now the variance depends on x through an x dependence in the stiffness k.

In the standard manner we can assume small dt and expand p around the current values of its arguments. After some simplification, we obtain

$$\frac{\partial p}{\partial t} = -\frac{\partial p}{\partial x} v\cos\Phi + \frac{\sigma(x)^2}{2}\frac{\partial^2 p}{\partial \Phi^2} + v\sin\Phi\frac{\partial}{\partial x}\left[\sigma(x)^2 dt\frac{\partial p}{\partial \Phi}\right].$$

The horizontal location x and moving direction Φ are directly coupled in the last term on the right-hand side, which is of the order of dt. We have checked that this third term can be neglected in our model, both in terms of any qualitative predictions but also (and perhaps more surprisingly) at little cost in quantitative accuracy even though our model involves discrete update steps. Consequently, Eq. (9) can be simplified to

$$\frac{\partial p}{\partial t} = -\frac{\partial p}{\partial x} v\cos(\Phi) + \frac{\sigma(x)^2}{2}\frac{\partial^2 p}{\partial \Phi^2}. \tag{9}$$

Following standard procedures (see, for example, Ref. [30]), one can show the Langevin equations below are equivalent to the Fokker-Planck approach:

$$\frac{dx}{dt} = v\cos(\Phi),$$
$$\frac{d\Phi}{dt} = \eta(t), \tag{10}$$

where $\langle\eta(t)\rangle = 0$ and $\langle\eta(t)\eta(t')\rangle = \delta(t - t')\sigma(x)^2$.

We then solve Eq. (9) for both the uniform and stiffness gradient substrate cases. Figure 4(a) shows the initial condition in the all cases discussed in the following; in particular we apply a narrow Gaussian distribution to approximate the δ in $p(x,\Phi;t = 0) = \frac{1}{2\pi}\delta(x)$, $\Phi \in (0,2\pi)$. The solution shows a peak in x that varies from being at positive values (for $\Phi \simeq 0$) to negative ones (for $\Phi \simeq \pi$); the peak heights are independent of Φ as expected via rotational symmetry [see Fig. 4(b)].

For the stiffness gradient case, the stiffness distribution is described by Eq. (5) with $L = 400$. The full distributions are shown at several times in Figs. 5(a) and 5(b). Now there is a

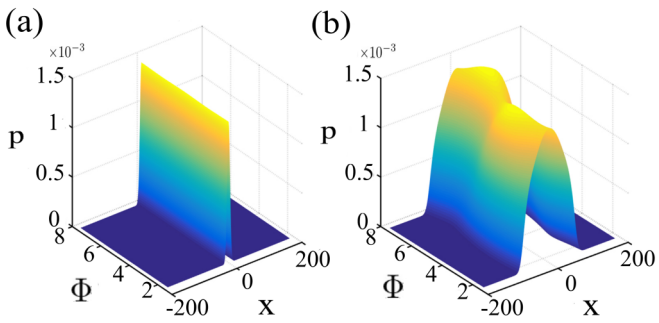

FIG. 4. The PDE solution. (a) Initial probability density function $p(x,\Phi;t=0)$. (b) Probability density function $p(x,\Phi;t=94)$ on a uniform substrate. Note that in this and the subsequent figure Φ runs from $\pi/2$ to $5\pi/2$.

clear peak as a function of the direction. Most cells adapt their moving directions from their initial directions $\Phi(t=0)$ to Φ near zero, exhibiting durotaxis (data not shown); this can be seen by showing a full 2D density plot, where there is a sharp ridge of cells moving ahead and a significant smearing of cells that are going backward [Fig. 5(c)]. This can be studied by defining $\hat{p}(x,t)=\int_0^{2\pi} p(x,\Phi,t)d\Phi$ and comparing our partial differential equation (PDE) result for this quantity with direct simulations [Fig. 5(d)]. The very good agreement between PDE and direct simulation results validates the Fokker-Planck equation approach. Note that as time progresses the above trends continue, with the population continuing to break up into a peak at positive x and a straggler peak at negative x corresponding to cells that have wandered out to the uniform less stiff side of the gradient profile.

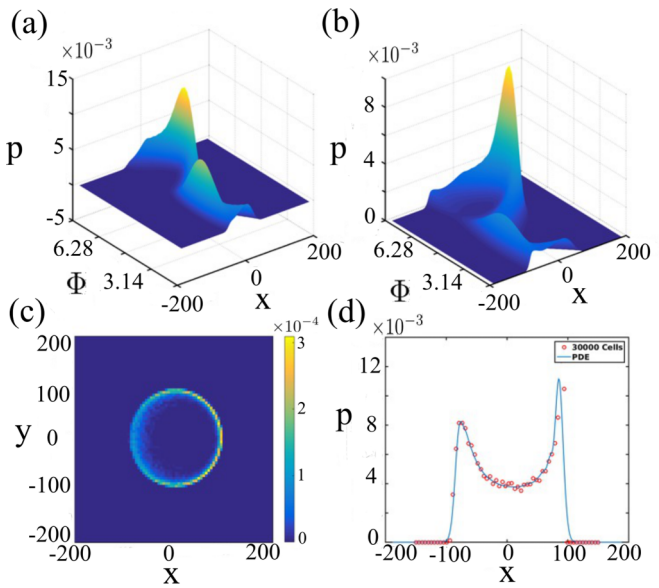

FIG. 5. The PDE solution and comparison to simulation on a substrate with stiffness gradient. Probability density distribution $p(x,\Phi;t)$ at (a) $t=56$ and (b) $t=94$. (c) Full 2D density plot from direct simulation. (d) Comparison between direct simulations of 30 000 cells and the numerical solution of the Fokker-Planck equation for $\hat{p}(x,t=94)$.

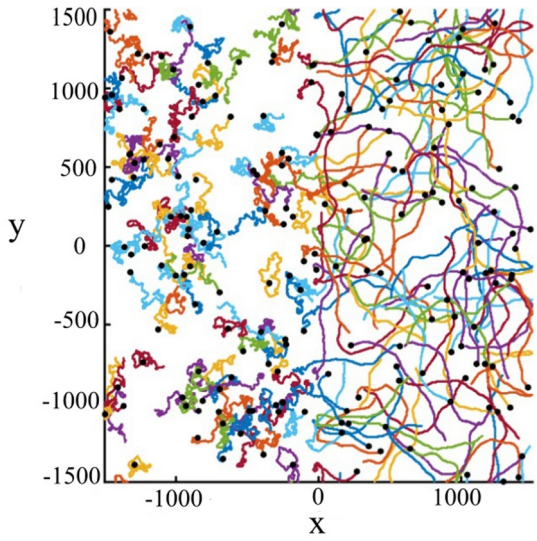

FIG. 6. Direct simulations with random initial velocities and uniform initial spatial density.

In general, the Fokker-Planck approach is computationally preferable, especially if we are interested in the long-time behavior of the density. With direct simulation, we often need to calculate many thousands of cells to determine a smooth distribution. An example is shown in Fig. 6(a), where the left side of the box is soft, the right half is hard, and we have used reflective boundary conditions in the x direction and periodic in the y direction. Even though the trajectories are very different on each side, the overall steady-state density distribution is flat (see Fig. 6). This can be obtained directly from the steady-state Fokker-Planck approach, either by numerical relaxation or analytically by separation of variables.

To see one last nontrivial use of the PDE approach, we now generalize our model to allow the velocity to be stiffness dependent. The Fokker-Planck equation now becomes

$$\frac{\partial p}{\partial t}=-\cos(\Phi)\frac{\partial}{\partial x}[pv(x)]+\frac{\sigma(x)^2}{2}\frac{\partial^2 p}{\partial \Phi^2}. \qquad (11)$$

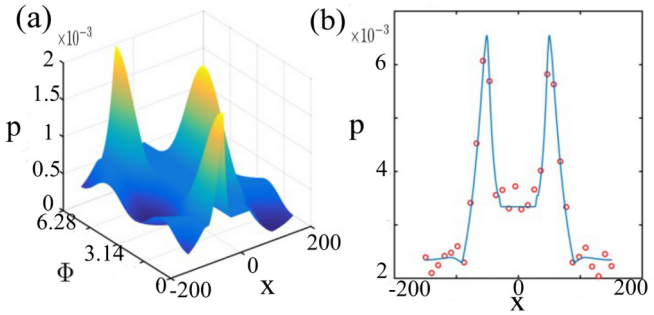

FIG. 7. Further test of the PDE. (a) Full PDE solution for periodic variation in stiffness and concomitant cell speed, with random initial velocities and uniform initial spatial density. (b) Comparison between direct simulations of 10 000 cells and the numerical solution of the Fokker-Planck equation for $\hat{p}(x,t=200)$.

We use the specific forms

$$k(x) = \begin{cases} k_{\text{hard}} = 5, & -150 < x < -90 \\ k_{\text{hard}} + \frac{k_{\text{soft}} - k_{\text{hard}}}{60}(X + 90), & -90 \leqslant X \leqslant -30 \\ k_{\text{soft}} = 1, & -30 < x < 30 \\ k_{\text{soft}} + \frac{k_{\text{hard}} - k_{\text{soft}}}{60}(X - 30), & 30 \leqslant X \leqslant 90 \\ k_{\text{hard}} = 5, & 90 < x < 150 \end{cases} \tag{12}$$

and for the same regions,

$$v(x) = \begin{cases} v_{\text{hard}} = 0.56, & -150 < x < -90 \\ \left(\frac{\sqrt{v_{\text{soft}}} - \sqrt{v_{\text{hard}}}}{60} \cdot (x + 90) + \sqrt{v_{\text{hard}}}\right)^2, & -90 \leqslant X \leqslant -30 \\ v_{\text{soft}} = 0.0165, & -30 < x < 30 \\ \left(\frac{-\sqrt{v_{\text{soft}}} + \sqrt{v_{\text{hard}}}}{60} \cdot (x - 30) + \sqrt{v_{\text{soft}}}\right)^2, & 30 \leqslant X \leqslant 90 \\ v_{\text{hard}} = 0.56, & 90 < x < 150. \end{cases} \tag{13}$$

Figure 7 shows that the PDE result matches very well with direction simulation, but direction simulation needs a very large number of cells to get a smooth result.

In this study we discussed a possible underlying mechanism for durotaxis, namely, a stiffness dependence of FA formation and possible FA-dependent speed. It is known that FAs can dynamically sample rigidity to act as mechanosensors [25], but it remains elusive how FA formation can directly control cell motility. In previous work it was shown that stiffness-dependent persistence time leads to durotaxis [19]. In our work we proposed several biophysical mechanisms that can cause positive correlation between persistence time and/or distance and substrate stiffness. For example, we show that a model starting from the stiffness-dependent FA formation assumption can generate results consistent with those in [19]. In addition, we derived the corresponding 2D Fokker-Planck equation associated with our model and showed that it gives consistent numerical agreement with our simulations. To show an alternative application of our model, we predicted long-term durotaxis effects on cell density distribution in the presence of a spatially complex stiffness field. We found that the velocity dependence on stiffness can lead to cell trapping on soft materials. Our work can potentially help in predicting cell motility in more complex physiological environments such as those arising during cancer metastasis.

Our model implicitly assumes that cells are incompetent at sensing rigidity gradients without moving around. For chemotaxis, a close analog of durotaxis, a eukaryotic cell is capable of comparing chemical concentration between its two ends, even though a typical bacterium is not [31]. It is technically hard to test such an ability in durotaxis, mainly because the cytoskeleton is essential for both cell motility and mechanosensing. Recently it was shown that some cells can exhibit durotaxis as a cluster even if isolated constituent cells are ineffective [32]; in this case motion appears to not be necessary.

This work was supported by the National Science Foundation Center for Theoretical Biological Physics (Grant No. NSF PHY-1427654). H.L. was also supported by the Cancer Prevention Research Institute of Texas Scholar program of the State of Texas.

[1] N. Wang, J. P. Butler, and D. E. Ingber, Mechanotransduction across the cell surface and through the cytoskeleton, Science **260**, 1124 (1993).

[2] F. Guilak, D. M. Cohen, B. T. Estes, J. M. Gimble, W. Liedtke, and C. S. Chen, Control of stem cell fate by physical interactions with the extracellular matrix, Cell Stem Cell **5**, 17 (2009).

[3] J. S. Park, J. S. Chu, A. D. Tsou, R. Diop, Z. Tang, A. Wang, and S. Li, The effect of matrix stiffness on the differentiation of mesenchymal stem cells in response to TGF-β, Biomaterials **32**, 3921 (2011).

[4] N. D. Evans, C. Minelli, E. Gentleman, V. LaPointe, S. N. Patankar, M. Kallivretaki, X. Chen, C. J. Roberts, and M. M. Stevens, Substrate stiffness affects early differentiation events in embryonic stem cells, Eur. Cell Mater. **18**, e13 (2009).

[5] B. Trappmann, J. E. Gautrot, J. T. Connelly, D. G. T. Strange, Y. Li, M. L. Oyen, M. A. Cohen Stuart, H. Boehm, B. Li, V. Vogel, J. P. Spatz, F. M. Watt, and W. T. S. Huck, Extracellular-matrix tethering regulates stem-cell fate, Nat. Mater. **11**, 642 (2012).

[6] R. J. Pelham, Jr. and Y.-l. Wang, Cell locomotion and focal adhesions are regulated by substrate flexibility, Proc. Natl. Acad. Sci. USA **94**, 13661 (1997).

[7] T. Yeung, P. C. Georges, L. A. Flanagan, B. Marg, M. Ortiz, M. Funaki, N. Zahir, W. Ming, V. Weaver, and P. A. Janmey, Effects of substrate stiffness on cell morphology, cytoskeletal structure, and adhesion, Cell Motil. Cytoskeleton **60**, 24 (2005).

[8] C.-M. Lo, H.-B. Wang, M. Dembo, and Y.-l. Wang, Cell movement is guided by the rigidity of the substrate, Biophys. J. **79**, 144 (2000).

[9] L. Bollmann, D. E. Koser, R. Shahapure, H. O. B. Gautier, G. A. Holzapfel, G. Scarcelli, M. C. Gather, E. Ulbricht, and K. Franze, Microglia mechanics: Immune activation alters traction forces and durotaxis, Front. Cell. Neurosci. **9**, 363 (2015).

[10] M. Basan, J. Elgeti, E. Hannezo, W.-J. Rappel, and H. Levine, Alignment of cellular motility forces with tissue flow as a mechanism for efficient wound healing, Proc. Natl. Acad. Sci. USA **110**, 2452 (2013).

[11] V. P. Losick, D. T. Fox, and A. C. Spradling, Polyploidization and cell fusion contribute to wound healing in the adult drosophila epithelium, Curr. Biol. **23**, 2224 (2013).

[12] S. Huang and D. E. Ingber, Cell tension, matrix mechanics, and cancer development, Cancer Cell **8**, 175 (2005).

[13] S. K. Venkatesh, M. Yin, J. F. Glockner, N. Takahashi, P. A. Araoz, J. A. Talwalkar, and R. L. Ehman, MR elastography of liver tumors: Preliminary results, Am. J. Roentgenol. **190**, 1534 (2008).

[14] R. Sambeth and A. Baumgaertner, Autocatalytic Polymerization Generates Persistent Random Walk of Crawling Cells, Phys. Rev. Lett. **86**, 5196 (2001).

[15] S. Huang, C. P. Brangwynne, K. K. Parker, and D. E. Ingber, Symmetry-breaking in mammalian cell cohort migration during tissue pattern formation: Role of random-walk persistence, Cell Motil. Cytoskeleton **61**, 201 (2005).

[16] Z. Sadjadi, M. R. Shaebani, H. Rieger, and L. Santen, Persistent-random-walk approach to anomalous transport of self-propelled particles, Phys. Rev. E **91**, 062715 (2015).

[17] A. M. Reynolds, Can spontaneous cell movements be modelled as Lévy walks? Physica A **389**, 273 (2010).

[18] S. V. Buldyrev, A. L. Goldberger, S. Havlin, C.-K. Peng, M. Simons, and H. E. Stanley, Generalized Lévy-walk model for DNA nucleotide sequences, Phys. Rev. E **47**, 4514 (1993).

[19] E. A. Novikova, M. Raab, D. E. Discher, and C. Storm, Persistence-Driven Durotaxis: Generic, Directed Motility in Rigidity Gradients, Phys. Rev. Lett. **118**, 078103 (2017).

[20] O. T. Fackler and R. Grosse, Cell motility through plasma membrane blebbing, J. Cell Biol. **181**, 879 (2008).

[21] K. Keren, Cell motility: The integrating role of the plasma membrane, Eur. Biophys. J. **40**, 1013 (2011).

[22] V. E. Galkin, A. Orlova, and E. H. Egelman, Actin filaments as tension sensors, Curr. Biol. **22**, R96 (2012).

[23] P. K. Mattila and P. Lappalainen, Filopodia: Molecular architecture and cellular functions, Nat. Rev. Mol. Cell Biol. **9**, 446 (2008).

[24] D.-H. Kim and D. Wirtz, Focal adhesion size uniquely predicts cell migration, FASEB J. **27**, 1351 (2013).

[25] S. V. Plotnikov, A. M. Pasapera, B. Sabass, and C. M. Waterman, Force fluctuations within focal adhesions mediate ECM-rigidity sensing to guide directed cell migration, Cell **151**, 1513 (2012).

[26] L. Trichet, J. Le Digabel, R. J. Hawkins, S. R. K. Vedula, M. Gupta, C. Ribrault, P. Hersen, R. Voituriez, and B. Ladoux, Evidence of a large-scale mechanosensing mechanism for cellular adaptation to substrate stiffness, Proc. Natl. Acad. Sci. USA **109**, 6933 (2012).

[27] B. C. Isenberg, P. A. DiMilla, M. Walker, S. Kim, and J. Y. Wong, Vascular smooth muscle cell durotaxis depends on substrate stiffness gradient strength, Biophys. J. **97**, 1313 (2009).

[28] D. Shao, H. Levine, and W.-J. Rappel, Coupling actin flow, adhesion, and morphology in a computational cell motility model, Proc. Natl. Acad. Sci. USA **109**, 6851 (2012).

[29] M. Raab, J. Swift, P. C. D. P. Dingal, P. Shah, J.-W. Shin, and D. E. Discher, Crawling from soft to stiff matrix polarizes the cytoskeleton and phosphoregulates myosin-II heavy chain, J. Cell Biol. **199**, 669 (2012).

[30] R. Zwanzig, *Nonequilibrium Statistical Mechanics* (Oxford University Press, Oxford, 2001).

[31] G. Witzany and M. Nowacki, *Biocommunication of Ciliates* (Springer, Berlin, 2016).

[32] R. Sunyer, V. Conte, J. Escribano, A. Elosegui-Artola, A. Labernadie, L. Valon, D. Navajas, J. M. García-Aznar, J. J. Muñoz, P. Roca-Cusachs, and X. Trepat, Collective cell durotaxis emerges from long-range intercellular force transmission, Science **353**, 1157 (2016).